

A New Control Method for Grid-Connected PV System Based on Quasi-Z-Source Cascaded Multilevel Inverter Using Evolutionary Algorithm

Hamid Reza Mohammadi, Ali Akhavan

Department of Electrical Engineering, University of Kashan, Kashan, Iran

Article Info

Article history:

Received Aug 27, 2014

Revised Dec 2, 2014

Accepted Dec 25, 2014

Keyword:

Cascaded multilevel inverter

Particle swarm optimization

Photovoltaic system

Quasi-Z-source inverter

ABSTRACT

In this paper, a new control method for quasi-Z-source cascaded multilevel inverter based grid-connected photovoltaic (PV) system is proposed. The proposed method is capable of boosting the PV array voltage to a higher level and solves the imbalance problem of DC-link voltage in traditional cascaded H-bridge inverters. The proposed control system adjusts the grid injected current in phase with the grid voltage and achieves independent maximum power point tracking (MPPT) for the separate PV arrays. To achieve these goals, the proportional-integral (PI) controllers are employed for each module. For achieving the best performance, this paper presents an optimum approach to design the controller parameters using particle swarm optimization (PSO). The primary design goal is to obtain good response by minimizing the integral absolute error. Also, the transient response is guaranteed by minimizing the overshoot, settling time and rise time of the system response. The effectiveness of the new proposed control method has been verified through simulation studies based on a seven level quasi-Z-Source cascaded multilevel inverter.

Copyright © 2015 Institute of Advanced Engineering and Science.
All rights reserved.

Corresponding Author:

Hamid Reza Mohammadi,
Departement of Electrical Engineering,
University of Kashan,
Kashan, Iran.
Email: mohammadi@kashanu.ac.ir

1. INTRODUCTION

Photovoltaic (PV) power generation has a great potential to serve as a clean and inexhaustible renewable energy source. However, output power of the PV arrays is greatly affected by environmental conditions such as stochastic changes of the temperature and solar irradiance. In PV systems, extracting the maximum power of the PV array and current injection into the grid at unity power factor are necessary. In recent years, applying various multilevel inverter topologies to PV systems is getting more and more attention due to the large power-scale and high voltage demands. Among various topologies, cascaded H-bridge (CHB) inverter has unique advantages and has been identified as a suitable topology for transformerless, grid-connected PV systems [1]. Applying CHB inverter in the PV systems has some advantages such as the independent maximum power point tracking (MPPT) of each array. However, the DC-link voltage in each inverter module is not constant, because PV array voltage varies due to the changes of environmental conditions such as temperature and solar irradiation or partial shadows. These cases will cause an imbalance DC-link voltage among different H-bridge modules. Furthermore, in the conventional cascaded multilevel inverter (CMI) based PV system, each module is a buck inverter because the first component of the output AC voltage, always is lower than the input DC voltage. Therefore, an additional DC-DC boost converter is necessary to obtain the desired output voltage, if the input voltage is lower than the desired output voltage

and also, to balance the DC-link voltages. This DC-DC boost converter increases the complexity of the power and control circuit and reduces the efficiency [2].

In recent years, the Z-source inverter (ZSI) and quasi-Z-source inverter (QZSI) have been employed for PV power generation system due to some unique advantages and features. Unlike quasi Z-source inverter, ZSI has a discontinuous input current during the shoot-through state due to the blocking diode. Nowadays, quasi-Z-source cascaded multilevel inverter (QZS-CMI) based PV systems were proposed which inherits the advantages of traditional CMI while overcoming issues with imbalance DC-link voltages among independent modules and PV array voltage boost. References [3]-[4] present the various multi-carrier bipolar PWM techniques for QZS-CMI and [5] focused on the parameter design of the QZS-CMI. The phase shifted sinusoidal pulse width modulation (PS-SPWM) is used in [6] as a modulation scheme, but PV system has never been modeled in detail to design the controllers.

In this paper a new control method for a QZS-CMI based PV system is proposed. The control objectives are independent DC-link voltage control, independent MPPT control and current injection to the grid at unity power factor. The proportional-integral (PI) controllers are employed to control each QZS-CMI module. To achieve a high and fast performance, this paper presents an optimum approach to design PI parameters using particle swarm optimization (PSO) and also the PS-SPWM modulation scheme is used for the single phase QZS-CMI. This paper is organized as follows: Section 2 consists an overview of the system with proposed control strategy; Section 3 focuses on the system modeling and grid-connected control; design of the PI parameters using PSO is presented in section 4; the PS-SPWM modulation scheme is presented in section 5; the effectiveness of the proposed strategy is verified by simulation and comparison the results with the reference [2] in section 6; and finally, a conclusion is made in section 7.

2. QZS-CMI AND ITS CONTROL STRATEGY

The QZS-CMI based grid-connected PV system with the proposed control strategy is shown in Figure 1. Comparing to the conventional CMI module, an inductor-capacitor impedance network is included in the input stage of each module. This structure is used to synthesize DC voltage sources to generate $2n + 1$ staircase output waveform where, n is the number of independent PV array. The individual PV source is an array composed of identical PV panels in series and parallel.

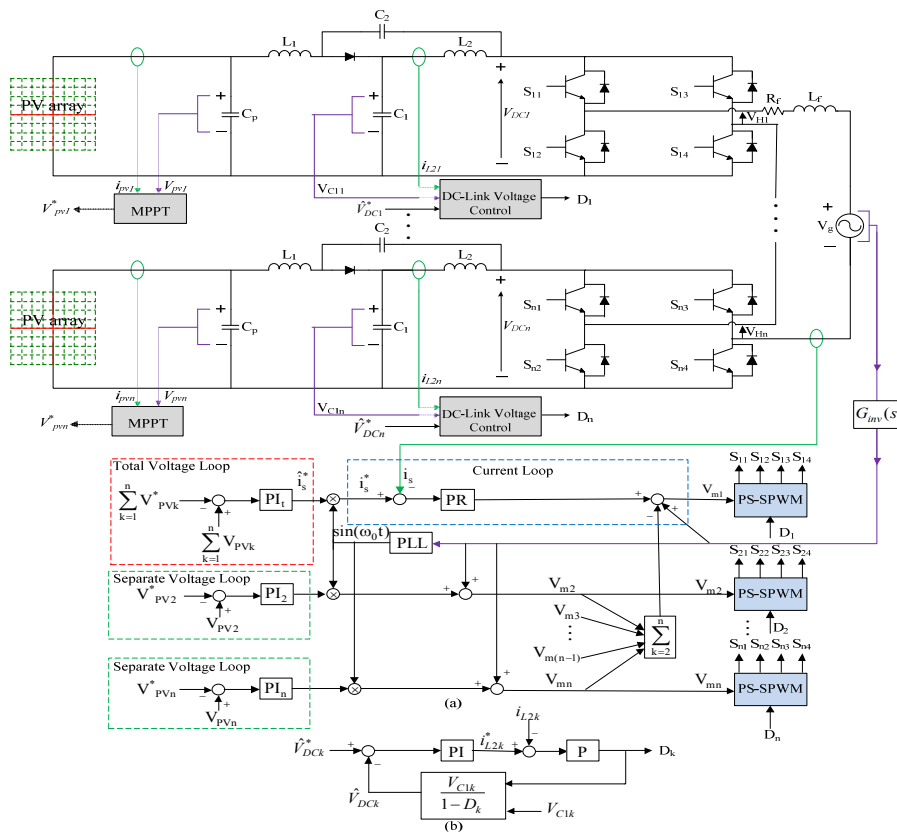


Figure 1. (a) qZS-CMI based grid-tie PV power system and (b) dc-link peak voltage control

2.1. Quasi-Z-source inverter operation

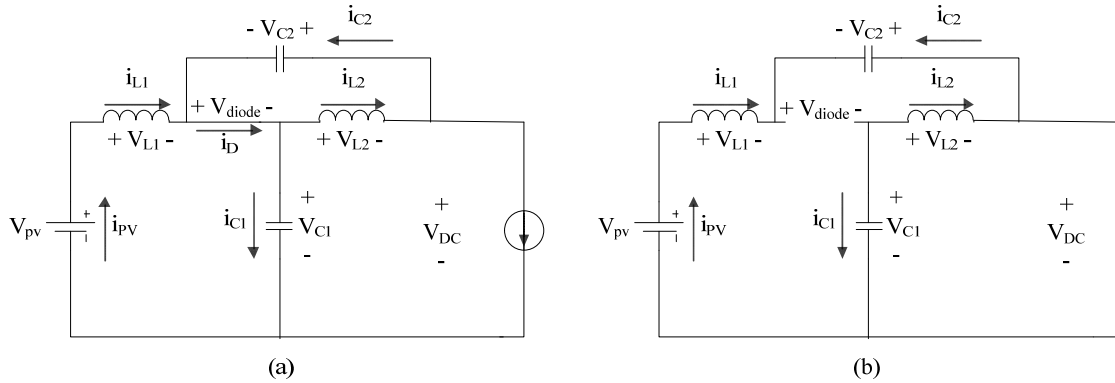


Figure 2. Equivalent circuit of the qZSI; (a) non-shoot-through state and (b) shoot-through state

The QZS-CMI combines the QZS network into each CMI module. The QZSI can be operated in two modes, i.e., the non-shoot-through and the shoot-through [6]. Figure 2 shows the QZSI equivalent circuits operating in the two modes and defines the polarities of all voltages and currents. If the switching period is T_s , the shoot-through period is T_{sh} and non-shoot-through period is T_{nsh} , where:

$$T_s = T_{sh} + T_{nsh} \quad (1)$$

Therefore, the shoot-through duty ratio is $D = T_{sh} / T_s$. When the k^{th} module is in non-shoot-through state, the power is transmitted from the DC side and inverter operates as a traditional CMI. In steady state, the following relations can be obtained.

$$\hat{V}_{DCk} = \frac{1}{1 - 2D_k} V_{PVk} = B_k V_{PVk} \quad , \quad V_{Hk} = S_k \hat{V}_{DCk} \quad (2)$$

While a shoot-through mode, there is no power transmission, because the DC-link voltage is zero. In this mode, there are:

$$\hat{V}_{DCk} = 0 \quad , \quad V_{Hk} = 0 \quad (3)$$

For the QZS-CMI, the synthesized voltage is:

$$V_H = \sum_{k=1}^n V_{Hk} = \sum_{k=1}^n S_k \hat{V}_{DCk} \quad (4)$$

In the above equations, \hat{V}_{DCk} is the k^{th} module DC-link peak voltage; V_{PVk} is the output voltage of the k^{th} PV array; D_k and B_k are the shoot-through duty ratio and boost factor of the k^{th} module, respectively; V_{Hk} is the output voltage of the k^{th} module and $S_k \in \{-1, 0, 1\}$ is the switching function of the k^{th} module.

2.2. Principle of Control Strategy

Each QZS-CMI module has two independent control commands: shoot-through duty ratio D_n and modulation signal V_m . D_n is used to adjust the DC-link voltage to a desired reference value. While, V_m is used to control the grid injected power. The main goals of the control system of QZS-CMI based grid-connected PV system are: 1) Independent MPPT for each module to ensure the maximum power extraction from each PV array; 2) Current injection into the grid at unity power factor and 3) Balance DC-link peak voltage for all QZS-CMI modules.

For achieving these goals, the PI controllers are employed. The total PV array voltage loop adjusts the sum of n PV array voltages using a PI controller, PI_v. Each PV array voltage reference is calculated by its MPPT block. Also, the current loop achieves a sinusoidal grid-injected current in phase with the grid voltage. A proportional-resonant (PR) controller makes the actual grid current to track the desired grid injected

current [7]. The $n-1$ independent PV array voltage loops control the other $n-1$ PV array voltages to achieve their own MPPTs through the $n-1$ PI controllers, named as PI_2 to PI_n , respectively. Also, as shown in Figure 1 (b), DC-link peak voltage is controlled in terms of its shoot-through duty ratio for each QZS-CMI module. A PI controller is used for the DC-link voltage loop to make the DC-link peak voltage tracks its reference value. A proportional controller (P) is used to improve the dynamic of the response. Finally, the independent shoot-through duty ratio D_k and modulation signal V_{mk} are combined into the PS-SPWM modulation scheme for k^{th} module to achieve the desired goals.

3. SYSTEM MODELING

The block diagram of the QZS-CMI based grid-connected PV system is shown in Figure 3. The details will be explained as follows.

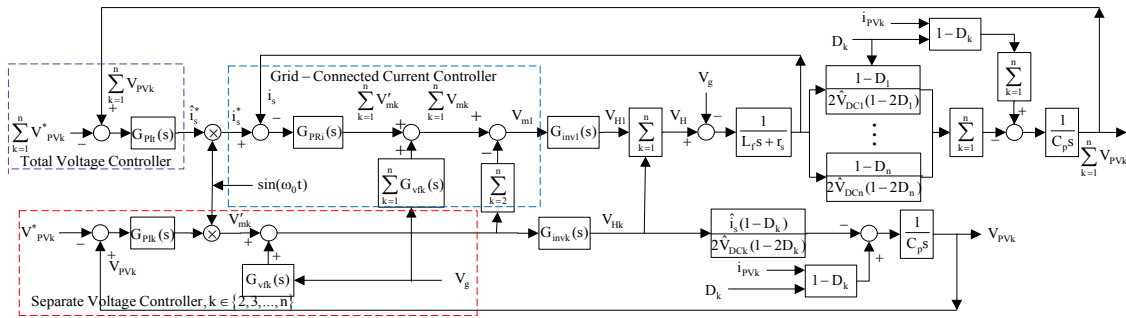


Figure 3. Block diagram of the proposed control grid-connected system for the QZS-CMI based PV system

3.1. Independent PV Voltage and Injected Current Control

In the k^{th} QZS-CMI module the current of the inductor L_I is:

$$i_{L1k} = i_{PVk} - C_p \frac{dV_{PVk}}{dt} \tag{5}$$

Where i_{L1k} is the current of inductor L_I and also, i_{PVk} is the current of k^{th} PV array; and C_p is the shunt capacitor with the PV array. The total output voltage of the QZS-CMI can be written as:

$$V_H = V_g + L_f \frac{di_s}{dt} + r_f i_s \tag{6}$$

Where V_g is the grid voltage and i_s is the grid injected current; r_f is parasitic resistance and L_f is the filter inductance. Consequently, the transfer function of the grid injected current can be obtained by:

$$G_f(s) = \frac{I_s(s)}{V_H(s) - V_g(s)} = \frac{1}{L_f s + r_f} \tag{7}$$

To make the actual grid injected current to track the desired reference, a PR controller $G_{PRI}(s) = k_{iP} + \frac{k_{iR} \omega_0}{s^2 + \omega_0^2}$ is used, where ω_0 is the resonant frequency i.e. 314 rad/s.

In the next step, a grid voltage feed forward control loop is applied. Therefore, the k^{th} module has the following modulation signal:

$$V_{mk} = V'_{mk} + V_g(s)G_{vfk}(s) \tag{8}$$

In the above equation, V_{mk} is the k^{th} module modulation signal; V'_{mk} is output of the PI controller in the k^{th} module and $G_{vfk}(s)$ is:

$$G_{V_{fjk}}(s) = \frac{1}{nG_{invk}(s)}, \quad G_{invk}(s) = \frac{V_{Hk}(s)}{V_{mk}(s)} = \hat{V}_{DCk} \quad (9)$$

Due to DC-link peak voltage balance control, the DC-link peak voltages are equal. Therefore:

$$G_{invk}(s) = G_{inv}(s), \quad k \in \{1, 2, \dots, n\} \quad (10)$$

According to Figure 3, the closed-loop transfer function of the grid injected current control system can be written as:

$$G_{ic} = \frac{I_s(s)}{I_s^*(s)} = \frac{G_{PRi}(s)G_f(s)G_{inv}(s)}{1 + G_{PRi}(s)G_f(s)G_{inv}(s)} = \frac{\hat{V}_{DCk}(k_{iP}S^2 + k_{iR}\omega_0^2)}{L_f S^3 + (r_f + \hat{V}_{DCk}k_{iP})S^2 + L_f\omega_0^2 S + \hat{V}_{DCk}k_{iR}\omega_0^2 + r_f\omega_0^2} \quad (11)$$

According to Figure 2, each PV array voltage can be obtained by:

$$V_{PVk}(s) = \frac{1}{C_p s} [I_{PVk}(s) - I_{L1k}(s)] \quad (12)$$

In the non-shoot-through mode, the output power is equal to input power. Therefore:

$$\frac{\hat{i}_s \hat{V}_{Hk}}{2} = \hat{v}_{DCk} \bar{i}_{DCk} = v_{PVk} \bar{i}_{L1k_nsh} \quad (13)$$

In the above equation, \hat{v}_{Hk} is the output peak voltage of the k^{th} module; \bar{i}_{DCk} is the average current of the DC-link in the k^{th} module; \bar{i}_{L1k_nsh} is the average current of inductor L_1 in non-shoot-through mode. Equation (13) can be rewritten using (2) as follows:

$$\bar{i}_{L1k_nsh} = \frac{\hat{i}_s \hat{V}_{Hk}}{2\hat{v}_{DCk}(1-2D_k)} \quad (14)$$

Also, in the shoot-through mode, the average current of the inductor L_1 is:

$$\bar{i}_{L1k_sh} = i_{PVk} \quad (15)$$

Therefore, the average current of the inductor L_1 in the one switching cycle can be obtained as follows:

$$\bar{i}_{L1k} = D_k \bar{i}_{L1k_sh} + (1-D_k) \bar{i}_{L1k_nsh} = D_k i_{PVk} + \frac{\hat{i}_s (1-D_k) \hat{V}_{Hk}}{2\hat{v}_{DCk}(1-2D_k)} \quad (16)$$

In addition, a PI controller $G_{PI}(s) = k_{PI} + \frac{k_{I}}{s}$ is used to track the total reference voltage coming from MPPT. The block diagram of the total PV array voltage loop is shown in Figure 4. Also, for modules 2 to n a PI controller $G_{PIk}(s) = k_{PIk} + \frac{k_{Ik}}{s}$ is applied to separate PV voltage to achieve their own MPPTs. The block diagram of the separate PV array voltage loop is shown in Figure 5.

3.2. Independent DC-link Voltage Control

The independent DC-link voltage control scheme is shown in Figure 1 (b). This control loop, adjust DC-link peak voltage using the capacitor- C_1 voltage and the inductor- L_2 current for each QZS-CMI module. Reference [8] presents the k^{th} QZS-CMI module's transfer function from the shoot-through duty ratio to the DC-link peak voltage, $G_{V_{dk}}(s)$ and from the shoot-through duty ratio to the inductor- L_2 current, $G_{i_{L2k}}(s)$ as follows:

$$G_{V_{dk}}(s) = \frac{\left(\frac{L}{1-2D_k} \hat{i}_s\right)s + (1-2D_k)(V_{ck1} + V_{ck2})}{LCs^2 + (R+r)Cs + (1-2D_k)^2} \tag{17}$$

$$G_{i_{Ldk}}(s) = \frac{LC(V_{ck1} + V_{ck2})s^2 + (R+r)(V_{ck1} + V_{ck2})Cs + (Ls + R + r)\frac{\hat{i}_s}{(1-2D_k)}}{(Ls + R + r)[LCs^2 + (R+r)Cs + (1-2D_k)^2]} \tag{18}$$

Where, L is the inductor and C is the capacitor of the impedance network. R is the series resistance of capacitors and r is the parasitic resistance of inductors; V_{ck1} and V_{ck2} are capacitor C_1 and C_2 voltages, respectively.

A proportional gain K_{dPk} is employed for the inductor current loop to improve the dynamic response. As shown in Figure 6, A PI controller with the transfer function of $G_{viPlk}(s) = k_{VdPk} + \frac{k_{VdIk}}{s}$ is cascaded to the inductor current loop to control the DC-link peak voltage.

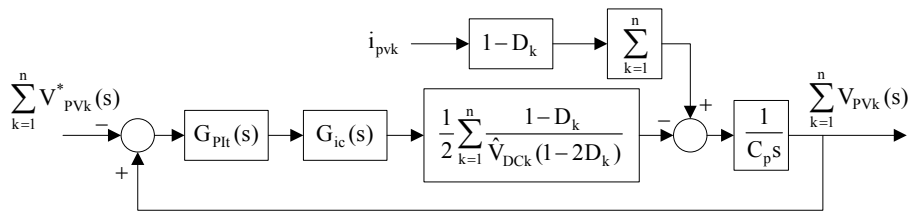


Figure 4. Block diagram of the total PV voltage loop

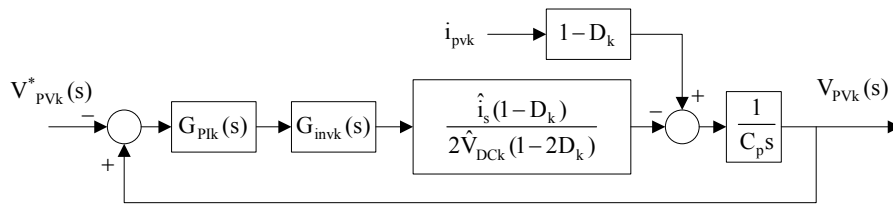


Figure 5. Block diagram of the separate PV voltage loop

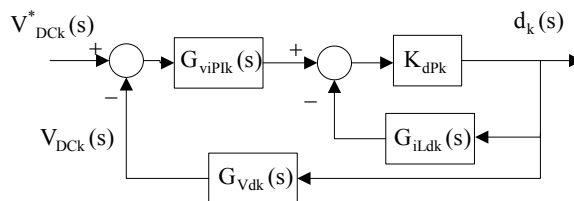


Figure 6. Block diagram of the DC-link peak voltage control of the k^{th} module

4. DESIGN OF PI CONTROLLERS USING PARTICLE SWARM OPTIMIZATION

The PI controller is a well-known method for industrial control processes. This is due to its robust performance and simple structure in a wide range of operating conditions. Tuning of such a controller requires specification of two parameters: proportional gain K_p and integral gain K_i [9]. In the past, this problem has been handled by a trial and error technique. In this paper, the problem of the PI parameters tuning is formulated as an optimization problem. The problem formulation employs four performance indexes, i.e., the overshoot, the settling time, the rise time and the integral absolute error of the step response as the objective function to tuning the PI parameters for getting a well performance under a given plant. In this study, the primary design goal is to obtain good response by minimizing the integral absolute error. At

the same time, the transient response is guaranteed by minimizing the overshoot, the settling time and the rise time of the step response. Furthermore, we employ a solution algorithm based on particle swarm optimization.

The PSO is a stochastic optimization technique, which uses swarming behaviors observed in flock of birds. In fact, the PSO was inspired by the sociological behavior associated with swarms. PSO was developed by James Kennedy and Russell Eberhart in 1995 as a new heuristic method [10]. It uses a number of particles that constitute a swarm moving around in one N -dimensional search space looking for the best position. The individuals in the swarm are called particles. Each particle in the PSO algorithm is a potential solution for the optimization problem and keep track of its co-ordinates in the problem space and tries to search the best position through flying in a multidimensional space, which are associated with the best solution (called best fitness) it has achieved so far that called "*pbest*". Another "best" value called "*gbest*" that is tracked by the global version of the particle swarm optimizer is the overall best value and its location obtained so far by each particle.

The transient response is very important, therefore both the amplitude and time duration of the transient response must be kept within tolerable limits. Hence, four indexes of the transient response are utilized to characterize the performance of PI control systems.

4.1. Response Parameters

Overshoot:

With the assumption of y as the step response, y_{max} is the maximum value and y_{ss} is the steady-state value of y . therefore the overshoot (f_O) is equal to:

$$f_O = y_{max} - y_{ss} \quad (19)$$

Rise Time:

The rise time (f_{RT}) is defined as the time required for the step response to rise from 10% to 90% of its final value. Hence:

$$f_{RT} = t_{y90\%} - t_{y10\%} \quad (20)$$

Settling Time:

The settling time (f_{ST}) is defined as the time required for the step response to decrease and stay within a 5% of its final value.

$$f_{ST} = t_{st} \quad (21)$$

Integral Absolute Error:

The integral absolute error (f_{IAE}) can be written as:

$$f_{IAE} = \int_0^{\infty} |e(t)| dt \quad (22)$$

4.2. Objective Function

The objective function (f_{Total}) for optimal design of PI controllers can be formulated as follows:

$$f_{Total} = f_O + f_{RT} + f_{ST} + f_{IAE} \quad (23)$$

To apply PSO for tuning the PI controllers, the closed-loop transfer function of the total PV voltage loop, separate PV voltage loop and DC-link peak voltage is necessary. These closed-loop transfer functions are calculated using block diagram of Figure 4–6, respectively.

$$\frac{\sum V_{PVk}}{\sum V_{PVk}^*} = \frac{\left[k_{P_i} k_{iP} s^3 + k_{i_i} k_{iP} s^2 + k_{P_i} (k_{iP} \omega_0^2 + k_{iR} \omega_0) s + k_{i_i} (k_{iP} \omega_0^2 + k_{iR} \omega_0) \right] \times \left(\frac{1-D_1}{2(1-2D_1)} + \frac{1-D_2}{2(1-2D_2)} + \frac{1-D_3}{2(1-2D_3)} \right)}{C_p L_f s^5 + C_p (\hat{V}_{DC} k_{iP} + r_f) s^4 + (C_p L_f \omega_0^2 + k_{P_i} k_{iP} \times \left(\frac{1-D_1}{2(1-2D_1)} + \frac{1-D_2}{2(1-2D_2)} + \frac{1-D_3}{2(1-2D_3)} \right)) s^3 + (C_p (\hat{V}_{DC} k_{iP} \omega_0^2 + \hat{V}_{DC} k_{iR} \omega_0 + r_f \omega_0^2) + k_{i_i} k_{iP} \left(\frac{1-D_1}{2(1-2D_1)} + \frac{1-D_2}{2(1-2D_2)} + \frac{1-D_3}{2(1-2D_3)} \right)) s^2 + k_{P_i} (k_{iP} \omega_0^2 + k_{iR} \omega_0) \left(\frac{1-D_1}{2(1-2D_1)} + \frac{1-D_2}{2(1-2D_2)} + \frac{1-D_3}{2(1-2D_3)} \right) s + k_{i_i} (k_{iP} \omega_0^2 + k_{iR} \omega_0) \left(\frac{1-D_1}{2(1-2D_1)} + \frac{1-D_2}{2(1-2D_2)} + \frac{1-D_3}{2(1-2D_3)} \right)}$$

$$\frac{V_{PVk}}{V_{PVk}^*} = \frac{k_{P_k} \left(\frac{1-D_k}{1-2D_k} \right) \frac{i_s}{2} s + k_{i_k} \left(\frac{1-D_k}{1-2D_k} \right) \frac{i_s}{2}}{C_p s^2 + k_{P_k} \left(\frac{1-D_k}{1-2D_k} \right) \frac{i_s}{2} s + k_{i_k} \left(\frac{1-D_k}{1-2D_k} \right) \frac{i_s}{2}}$$

$$\frac{d_k(s)}{V_{DCk}^*(s)} =$$

$$\frac{k_{V_{dPk}} L^2 C s^5 + k_{dPk} k_{V_{dPk}} (LC(R+r) + LC) s^4 + k_{V_{dIk}} k_{dPk} L^2 C s^3 + (k_{dPk} k_{V_{dPk}} (R+r)(1-2D_k)^2 s^2 + (Lk_{dPk} \frac{\hat{i}_s}{1-2D_k}) s + k_{dPk} k_{V_{dPk}} (R+r))}{L^2 C s^6 + LC(R+r) s^5 + (LCk_{dPk} \hat{V}_{DCk}) s^4 + (L(1-2D_k)^2 + (R+r)^2) s^3 + (k_{dPk} (R+r) C \hat{V}_{DCk}) s^2 + (R+r)^2 s + k_{dPk} k_{V_{dIk}} (1-2D_k)^2}$$

5. THE PS-SPWM FOR QZS-CMI

The modulation technique applied in the proposed system is a phase shifted sinusoidal pulse width modulation that shown in Figure 7. The shoot-through states are inserted with the simple boost control method. In this control method, two straight lines, which are denoted as $1-D_n$ and D_n-1 , envelopes equal to or greater than the peak value of the sinusoidal reference signals are used to control shoot-through duty ratio.

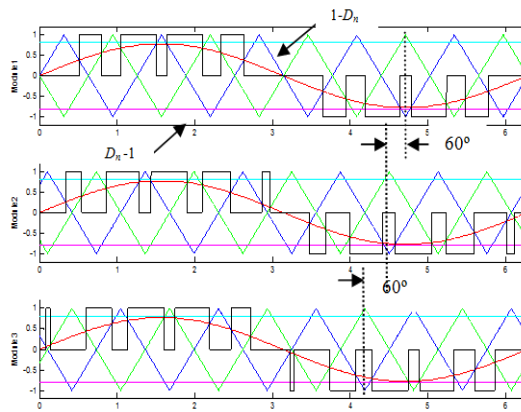


Figure 7. Modulation scheme for the proposed system

If the triangular carrier signal is smaller than D_n-1 or bigger than $1-D_n$ the two switches of one leg in H-bridge module are turned on simultaneously [6]. In PS-SPWM schemes, the number of triangular carrier waves is equal to $m-1$, where m is the level number. Also, the required phase shifts among different carriers is given as:

$$\varphi = \frac{360^\circ}{m-1}$$

Therefore, in this case ($m=7$) triangular carriers of different H-bridge modules are shifted 60° with respect to each other.

6. SIMULATION RESULTS

The performance evaluation of the proposed control strategy was carried out by different simulation in PSCAD/EMTDC. The parameters of the QZS-CMI are shown in Table 1. Also the PSO algorithm is programmed in MATLAB to obtain the best parameters for the PR and PI controllers. As mentioned earlier, the closed-loop transfer function of the total PV voltage control loop, the separate PV voltage control loop and the DC-link peak voltage control loop are used for optimization problem. The results of the PSO algorithm are shown in Table 2. The effectiveness of the proposed method is shown by comparing the results of the new proposed method for parameter tuning of PI controllers with the results of [2] in Table 3. In this table, the overshoot, the settling time and the rise time of the step response for these closed-loop transfer functions are presented. As shown in this table, the overshoot, the settling time and the rise time of step response for all the closed-loop transfer functions obtained using PSO algorithm is smaller than the results of [2].

Table 1. QZS-CMI Parameters

QZS-CMI Parameters	Value
QZS inductance, L_1 and L_2	1.8 mH
QZS capacitance, C_1 and C_2	3300 μ F
PV array parallel capacitance, C_p	1100 μ F
Filter inductance, L_f	1mH
Carrier frequency, f_c	5kHz
Grid voltage	220V/50Hz

Table 2. The Parameters of the Control System by Pso Algorithm

Parameters	Value	Parameters	Value
k_{iP}	0.00491	k_{iR}	-0.01673
k_{P_t}	1.1511	k_{I_t}	1.5348
k_{Pk}	0.0263	k_{Ik}	0.0017
k_{dPk}	0.0073		
k_{VdPk}	0.0313	k_{VdIk}	2.8122

Table 3. Transfer Functions Characteristics

Transfer functions	Overshoot (%)		Settling time (sec)		Rise time (sec)	
	using PSO data	using [2] data	using PSO data	using [2] data	using PSO data	using [2] data
Total PV voltage loop	8.62	56.1	0.362	2.84	0.0395	0.177
Separate PV voltage loop	12.9	33.3	0.438	0.511	0.0578	0.0651
DC-link peak voltage loop	≈ 0	≈ 0	0.243	1.38	0.13	0.779

The P-V characteristic of the PV array is shown in Figure 8. The measured voltage and current of each PV array are used to calculate the MPPT search algorithm for the PV voltage reference at the MPP. Incremental conductance algorithm is used for tracking the maximum power point of a PV array in this paper [11].

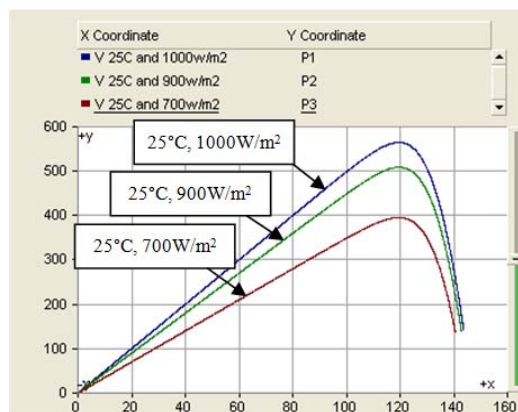


Figure 8. PV array power-voltage characteristic

At first, all modules are working at 1000 W/m^2 and 25°C condition and all the initial voltage references of MPPT algorithm are given at 120 V. The peak value of DC-link voltage of all modules is controlled at 145V. After 1 second, the third module's irradiation decreases to 700 W/m^2 . Hence, according to Figure 8, the reference of MPPT decreases to about 119.3 V. It should be noted that, the change of temperature mostly affects the voltage of maximum power point, so that, temperature rising causes the voltage of maximum power point to drop. While the change of solar irradiation affects the current injection.

The total PV voltage (sum of all three PV array voltages) and other PV array voltages are shown in Figure 9(a)-(d), respectively. It can be seen that during the change in the MPPT reference value due to change of environmental condition, the proposed control method have excellent tracking performance after a very short transient. It can be seen in Figure 9(d) that, after a change in the environmental condition of module 3, the controller of this module tracks the new reference. While, module 2 have not any transient because no change is happening in its condition. As shown in Figure 9(b-d), PV array voltage of module 1 is different with respect to modules 2 and 3. This is due to the fact that the modulation signal generation of module 1 is different from other modules.

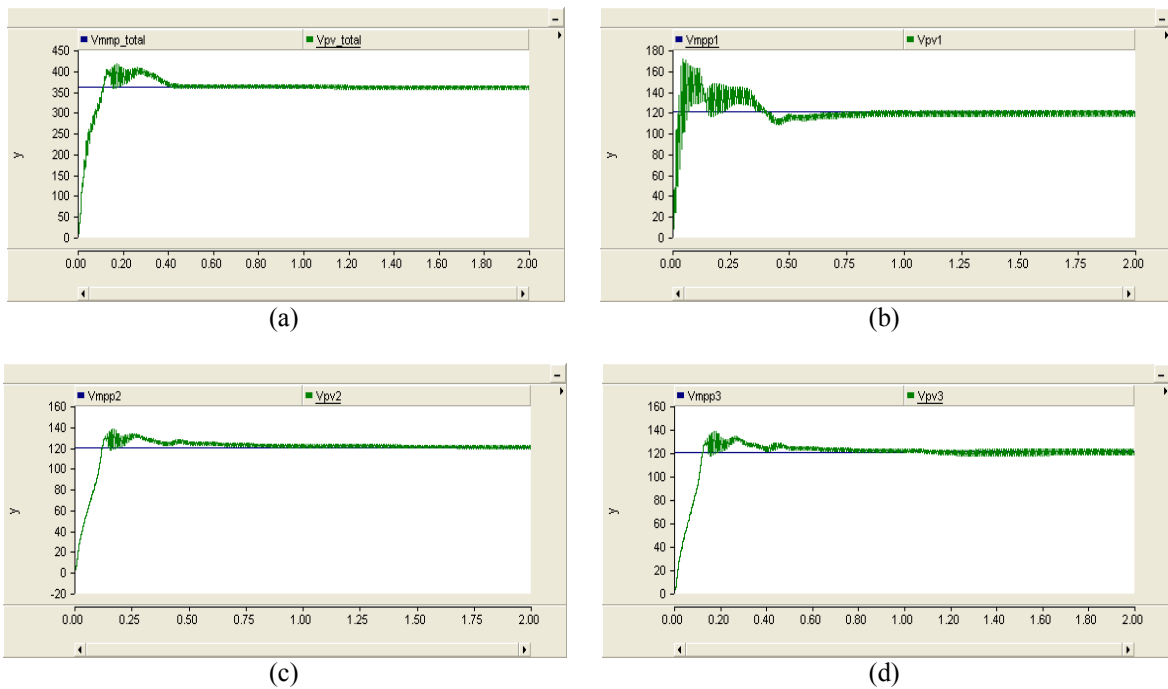


Figure 9. Simulation results (a) Total PV array voltage; (b) PV array voltage of module 1; (c) PV array voltage of module 2; (d) PV array voltage of module 3

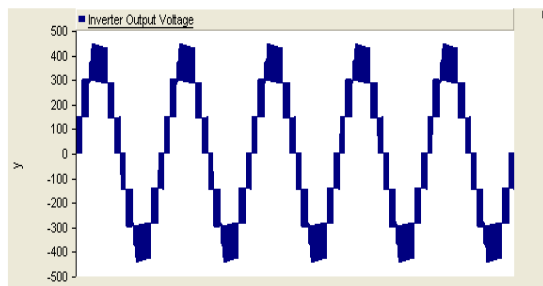


Figure 10. Inverter output voltage

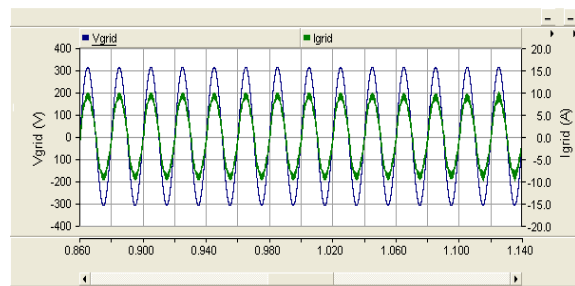


Figure 11. Grid voltage and current

The inverter output voltage is shown in Figure 10. It can be indicated that the solar irradiation or temperature does not affect the seven-level staircase output voltage of the inverter due to shoot-through

operation. It is no matter the temperature and the solar irradiation changes or not, the QZS-CMI always outputs a constant voltage, which verifies the voltage balancing capability.

Figure 11 shows the grid-injected current which is exactly in phase with the grid voltage and ensures unity power factor. It should be noted that, lower irradiation causes reduction of the grid-injected current as Figure 12, which the RMS value of the grid injected current is shown. As shown in this figure, the injected current reduces about 0.3A after reduction of irradiation.

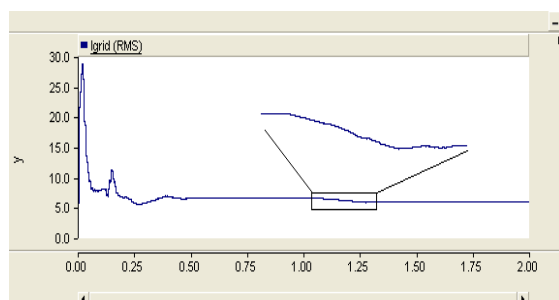


Figure 12. RMS value of the grid injected current

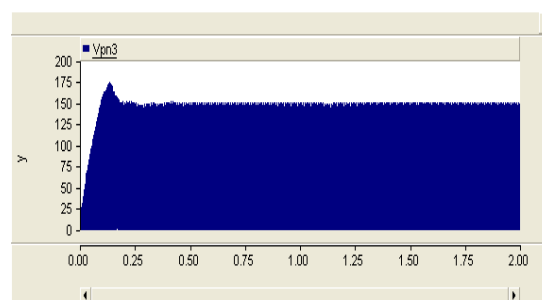


Figure 13. DC-link voltage of module 3

The DC-link voltage of module 3 is shown in Figure 13. It can be seen that, with the independent DC-link voltage control, DC-link peak voltage are kept at the reference value (145 V). It should be noted that, according to (2), after decrement of the MPPT reference value of module 3, longer shoot-through time interval is necessary for this module to fix the DC-link peak voltage at 145 V. As shown in Figure 13, DC-link peak voltage control loop, adjusts new shoot-through duty ratio after a very short transient, so that, third module's DC-link peak voltage have a very low distortion after a change in the solar irradiation.

7. CONCLUSION

This paper proposed a new control method for QZS-CMI based single-phase grid-connected PV system. The proposed system is a combination of QZSI and CHB multilevel topology and has both advantages of them. This enables independent MPPT control even if some modules' PV array had different conditions. Moreover, independent DC-link voltage control enforced all QZS-HBI modules have the balanced voltage and also, grid-injected current was fulfilled at unity power factor. The control parameters designed using PSO algorithm and it was shown that the system has fast and accurate response. A PS-SPWM technique was proposed for modulation to synthesize the staircase voltage waveform of the single-phase QZS-CMI. A simulation was carried out on a seven level QZS-CMI in the variable environmental condition. The simulation results show the effectiveness of the proposed control strategy for a QZS-CMI based single-phase grid-connected PV system.

REFERENCES

- [1] J Sastry, P Bakas, H Kim, L Wang, A Marinopoulos. Evaluation of cascaded H-bridge inverter for utility-scale photovoltaic systems. *Renewable Energy*. 2014; 69: 208-218.
- [2] Y Liu, B Ge, H Abu-Rub, FZ Peng. An Effective Control Method for Quasi-Z-Source Cascade Multilevel Inverter-Based Grid-Tie Single-Phase Photovoltaic Power System. *IEEE Transactions on Industrial Informatics*. 2014; 10(1): 399-407.
- [3] I Colak, E Kabalci, R Bayindir. Review of multilevel voltage source inverter topologies and control schemes. *Energy Conversion and Management*. 2011; 52(2): 1114-1128.
- [4] Y Liu, H Abu-Rub, B Ge, FZ Peng. Phase-shifted pulse-width-amplitude modulation for quasi-Z-source cascade multilevel inverter based PV power system. *Energy Conversion Congress and Exposition (ECCE), IEEE*. 2013; 94-100.
- [5] D Sun, B Ge, X Yan, D Bi, H Zhang, Y Liu, H Abu-Rub, L BenBrahim, F Peng. Modeling, Impedance Design, and Efficiency Analysis of Quasi-Z Source Module in Cascade Multilevel Photovoltaic Power System. *IEEE Transactions on Industrial Electronics*. 2014; 61(11): 6108-6117.
- [6] D Sun, B Ge, FZ Peng, AR Haitham, D Bi, Y Liu. A new grid-connected PV system based on cascaded H-bridge quasi-Z source inverter. *IEEE International Symposium on Industrial Electronics (ISIE2012)*. 2012; 951,956.
- [7] DN Zmood, DG Holmes. Stationary frame current regulation of PWM inverters with zero steady-state error. *IEEE Transactions on Power Electronics*. 2003; 18(3): 814,822.

-
- [8] Y Liu, B Ge, FZ Peng, AR Haitham, AT de Almeida, Ferreira FJTE. Quasi-Z-Source inverter based PMSG wind power generation system. *Energy Conversion Congress and Exposition (ECCE), IEEE*. 2011; 291-297.
 - [9] YT Hsiao, CL Chuang, CC Chien. Ant colony optimization for designing of PID controllers. *IEEE International Symposium on Computer Aided Control Systems Design*. 2004; 321-326.
 - [10] J Kennedy, R Eberhart. Particle swarm optimization. *IEEE International Conference on Neural Networks*. 1995; 1942-1948.
 - [11] V Salas, E Olías, A Barrado, A Lázaro. Review of the maximum power point tracking algorithms for stand-alone photovoltaic systems. *Solar Energy Materials and Solar Cells*. 2006; 90(11); 1555-1578.